Journal of Solid State Chemistry 184 (2011) 2075–2082

Contents lists available at ScienceDirect

Journal of Solid State Chemistry

journal homepage: www.elsevier.com/locate/jssc

Magnetostructural correlations in the antiferromagnetic $Co_{2-x}Cu_x(OH)AsO_4$ ($x=0$ and 0.3) phases

I. de Pedro [a,b,*], J.M. Rojo [a], J.L. Pizarro [c], J. Rodríguez Fernández [b], M.I. Arriortua [c], T. Rojo [a]

[a] Departamento de Química Inorgánica, Facultad de Ciencia y Tecnología, Universidad del País Vasco UPV/EHU, 48080 Bilbao, Spain
[b] CITIMAC, Facultad de Ciencias, Universidad de Cantabria, 39005 Santander, Spain
[c] Departamento de Mineralogía y Petrología, Facultad de Ciencia y Tecnología, Universidad del País Vasco UPV/EHU, 48080 Bilbao, Spain

ARTICLE INFO

Article history:
Received 20 January 2011
Received in revised form
23 May 2011
Accepted 29 May 2011
Available online 13 June 2011

Keywords:
Cobalt-copper hydroxi-arsenate
Hydrothermal synthesis
Crystal structure
Heat capacity
Magnetic properties

ABSTRACT

The $Co_{2-x}Cu_x(OH)AsO_4$ ($x=0$ and 0.3) compounds have been synthesized under mild hydrothermal conditions and characterized by X-ray single-crystal diffraction and spectroscopic data. The hydroxi-arsenate phases crystallize in the *Pnnm* orthorhombic space group with $Z=4$ and the unit-cell parameters are $a=8.277(2)$ Å, $b=8.559(2)$ Å, $c=6.039(1)$ Å and $a=8.316(1)$ Å, $b=8.523(2)$ Å, $c=6.047(1)$ Å for $x=0$ and 0.3, respectively. The crystal structure consists of a three-dimensional framework in which $M(1)O_5$-trigonal bipyramid dimers and $M(2)O_6$-octahedral chains (M=Co and Cu) are present. $Co_2(OH)AsO_4$ shows an anomalous three-dimensional antiferromagnetic ordering influenced by the magnetic field below 21 K within the presence of a ferromagnetic component below the ordering temperature. When Co^{2+} is partially substituted by Cu^{2+} ions, $Co_{1.7}Cu_{0.3}(OH)AsO_4$, the ferromagnetic component observed in $Co_2(OH)AsO_4$ disappears and the antiferromagnetic order is maintained in the entire temperature range. Heat capacity measurements show an unusual magnetic field dependence of the antiferromagnetic transitions. This λ-type anomaly associated to the three-dimensional antiferromagnetic ordering grows with the magnetic field and becomes better defined as observed in the non-substituted phase. These results are attributed to the presence of the unpaired electron in the dx^2-y^2 orbital and the absence of overlap between neighbour ions.

1. Introduction

The chemistry of transition metal phosphate and arsenate minerals has been traditionally considered as an interesting field of research for solid-state physicists and chemists. Many natural or synthetic phases present structures, which can give rise to potential applications and original physical properties such as magnetic, heterogeneous catalysis, ion exchange, optical or thermal expansion [1–5]. For example, the natural or synthetic $Cu_2(OH)PO_4$ phosphate can be used as a good catalyst for the catalytic oxidation of organic substrates by H_2O_2 and both catalytic activity and selectivity in the oxidation of olefins and alcohols by molecular oxygen under air have been observed [6,7].

The adamite-type, $M_2(OH)XO_4$ [M=Zn, Mn, Co, Ni, Cu; Mg, Mn, etc.; X=P and As] [8–17] family, have been known as minerals for a long time but some of them have not been prepared in the laboratory as pure phases although different synthetic methods were used. Unfortunately, in many of these natural or synthetic phases, even if good crystals for X-ray structure determination were obtained, the study of physical–chemical properties has not been possible due to the presence of impurities or mixed phases [12–19]. The $M_2(OH)AsO_4$ crystal structure [20] consists of a condensed framework of a vertex and edge-sharing $|MO_6|$, $|MO_5|$ and $|AsO_4|$ subunits (see Fig. 1). In the structure the metal ions can be sited in two different topologies: the octahedral and trigonal bipyramidal. The edge-sharing $[M(2)O_4(OH)_2]$ octahedra give rise to linear chains propagated along the c axis whereas the edge-sharing $[M(1)O_4(OH)]$ trigonal bipyramids constitute dimeric entities. The chain of octahedral, the dimeric units, and the tetrahedral groups share corners, thereby forming a three-dimensional network. In the case of $Co_2(OH)AsO_4$, the structure was solved by Seller et al. [19] from single-crystal data but the final position of the hydrogen ions was not reported. Recently, neutron powder-diffraction measurements were performed to obtain both nuclear and magnetic structures of this compound and an interesting incommensurate–commensurate magnetic phase transition was observed [21].

As a part of our recent research in the magnetic behaviour of adamite-type compounds, we have observed that the cobalt-based $Co_2(OH)XO_4$ (X=P and As) compounds present fascinating magnetic phenomena for insulators [22]. For instance, coexistence in

* Corresponding author at: Departamento de Química Inorgánica, Facultad de Ciencia y Tecnología, Universidad del País Vasco UPV/EHU, 48080 Bilbao, Spain.
E-mail address: depedrovm@unican.es (I. de Pedro).

0022-4596/$ - see front matter © 2011 Elsevier Inc. All rights reserved.
doi:10.1016/j.jssc.2011.05.060

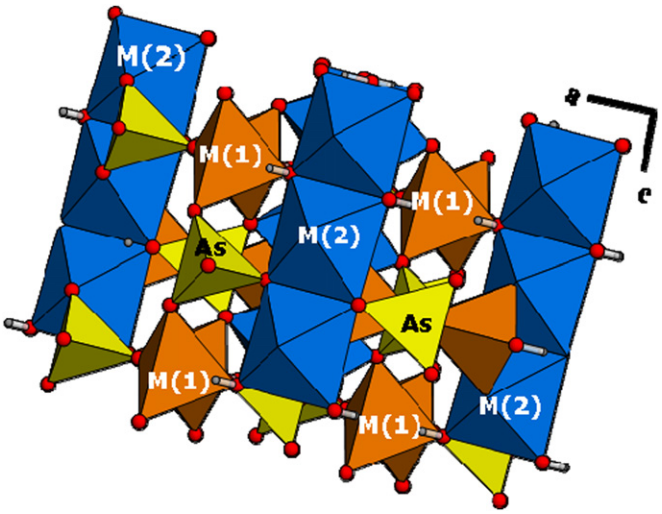

Fig. 1. Schematic drawing of the $Co_{2-x}Cu_x(OH)AsO_4$ ($x=0$ and 0.3) crystal structure view along the $|0\,1\,0|$ direction. Polyhedra are occupied by the M(II) ions (M=Co and Cu) and the AsO_4 groups are represented by tetrahedra. Big circles correspond to the oxygen atoms, and small circles show the hydrogen atoms.

the $Co_2(OH)PO_4$ magnetic frustration system of an antiferromagnetic ordering and a spin-glass behaviour at low temperatures [23], field-induced magnetic transitions in the $Co_2(OH)AsO_4$ phase [21] or evolution from commensurate to incommensurate antiferromagnetic structure in the $Co_2(OH)(PO_4)_{1-x}AsO_4)_x$ solid solution [24]. Furthermore, the partial substitution of transition metal ions in the non-substituted cobalt hydroxi-phosphate showed the evolution of a three-dimensional antiferromagnetic system in the $Co_{2-x}Cu_x(OH)PO_4$ solid solution [25] up to a spin-gap system in the $Cu_2(OH)PO_4$ phase [26], a spin-glass-like state in the $(Co,Ni)_2(OH)PO_4$ phases below 10 K [27] and higher ferromagnetic interactions at lower temperatures in $Co_{1.7}Mn_{0.3}(OH)PO_4$ coexisting with a similar spin-glass-like state [28]. As was observed in the homologous phosphate phase [25], the spin decompositions originated by the partial substitution of Co^{2+} ($S=3/2$) by Cu^{2+} ($S=1/2$) in the $Co_2(OH)AsO_4$ phase could give rise to interesting variations in their complex physical properties.

In this work, we report on the synthesis, single crystal structure, spectroscopic characterization and magnetic properties of a new cobalt–copper compound, $Co_{1.7}Cu_{0.3}(OH)AsO_4$, together with a comparative study with the isomorphous non-substituted $Co_2(OH)AsO_4$ phase.

2. Experimental

2.1. Synthesis and structural characterization

Recently, hydrothermal techniques have been successfully used to prepare hydroxi-arsenates of transition metal ions [26,29–32]. In this sense, the $Co_{2-x}Cu_x(OH)AsO_4$ ($x=0$ and 0.3) compounds were obtained starting from stoichiometric precursors, $(Co,Cu)_3(AsO_4)_2\cdot 8H_2O$, that were prepared following a synthetic method previously described [33]. Long reaction times were needed due to the low solubility of the hydrated arsenates. The mixtures were added to a volume of 100 mL of water/ammonia (~5%) and stirred up to homogeneity. The washed precursors were placed in a PTFE lined stainless steel pressure vessel and heated at 170 °C for 5 days, followed by slow cooling to room temperature. The pH of the mixtures did not show any appreciable change during the hydrothermal reactions and remained at approximately 7 for $x=0$, and 8 for $x=0.3$. In both compounds, blue single crystals together with similar colour powdered samples were obtained. The contents of cobalt, copper and arsenic were determined by inductively coupled plasma atomic emission spectroscopy (ICP AES) performed with an ARL Fisions 3410 spectrometer. The results were consistent with the $Co_{2-x}Cu_x(OH)AsO_4$ ($x=0$ and 0.3) stoichiometries.

The X-ray powder diffraction data were used to evaluate the purity of the arsenate products obtained in the synthesis. The powder diffraction patterns were recorded on a Panalytical X'Pert-MPD X-ray diffractometer in Bragg–Bentrano geometry, using graphite-monocromated Cu-$K\alpha$ radiation. The data collection took place in the 10–90° 2θ, every 0.02°, with 16 s per step. The data were fitted using the pattern matching routine of the programme FULLPROF [34], in orthorhombic cells with the *Pnnm* space group, as previously determined from single crystal data by Riffel et al. [20] for the $Co_2(OH)AsO_4$ phase. In the single-crystal X-ray diffraction, the data were collected at room temperature on an Oxford diffraction XCALIBUR2 using the graphite-monochromated Mo-$K\alpha$ radiation.

2.2. Physicochemical characterization techniques

The thermogravimetric (TGA) and differential thermal analysis (DTA) of $Co_{2-x}Cu_x(OH)AsO_4$ ($x=0$ and 0.3) were performed on a computer-controlled Perkin-Elmer TGA-DSC System 7 thermobalance. 20 mg of each sample were heated in air with a heating rate of 5 °C min^{-1} from 30 to 800 °C. The decomposition curves reveal an initial ($\approx$0.1% and 0.5% for $x=0$ and 0.3, respectively) weight loss associated with water absorbed on the surface from the atmosphere, and at 660 and 680 °C, respectively, a second step ($\approx$3.5% and 4.4%) attributed to the loss of water obtained from the decomposition of two formula units. The decomposition reaction can be described as follows:

$$2[Co_{2-x}Cu_x(OH)AsO_4]\rightarrow[1-(2x)]CoO+(2x)CuO+Co_3(AsO_4)_2+H_2O$$

At temperatures above 700 °C additional weight losses were not observed on the thermogravimetric curve. These results are in good agreement with those obtained for other hydroxi-phosphate and arsenate related compounds [23,25,30].

Spectroscopic measurements of $Co_{2-x}Cu_x(OH)AsO_4$ ($x=0$ and 0.3) were studied by both infrared and diffuse reflectance data. The IR spectra (KBr pellets) were obtained with a MATTSON 1000 FT-IT spectrometer in the 400–4000 cm^{-1} range. The absorbance spectra of the polycrystalline samples were registered at room temperature by diffuse reflectance technique on a Cary 2415 UV–vis-IR spectrometer in the 5000–50000 cm^{-1} range.

Magnetic susceptibility measurements of polycrystalline samples were performed using a Quantum Design MPSM-7 SQUID magnetometer whilst heating from 2 to 300 K in an applied magnetic field of 1 kOe, after cooling either in the presence (field cooling-FC) or absence (zero field cooling-ZFC) of the applied field. Magnetization as a function of field (H) was measured using the same MPSM-7 SQUID magnetometer in the range $-7\leq H/T\leq 7$ at 5 K after cooling the sample in zero field. Heat capacity measurements were carried out with a standard QD PPMS device by a traditional relaxation method using a two-tao model. The weight of the samples were 11.2 and 10.7 mg for $x=0$ and 0.3, respectively, obtained by compressing the original polycrystalline powder. In order to assure good thermal contact, the sample was glued to the sample-holder using Apiezon N grease. Data were collected with zero field and under an applied field of 90 kOe from 1.8 to 300 K. The addenda (sample-holder plus grease) was measured at different magnetic fields prior to the sample measurements and then subtracted from the total heat capacity in order to get the sample heat capacity.

2.3. Single-crystal X-ray diffraction

Prismatic single crystals of the $Co_{2-x}Cu_x(OH)AsO_4$ ($x=0$ and 0.3) compounds with dimensions $0.11\times0.07\times0.05$ and $0.13\times0.07\times0.05$ mm for $x=0$ and 0.3, respectively, were carefully selected under a polarizing microscope and mounted on glass fibre. Details of crystal data, intensity collection and some features of the structure refinement are reported in Table 1. 3083 reflections were measured for the cobalt hydroxi-arsenate phase in the range $4.93^\circ\le\theta\le26.04^\circ$, which were considered as independent 427 (R_{int} 0.0540) applying the criterion $I>2\ \sigma(I)$. For $Co_{1.7}Cu_{0.3}(OH)AsO_4$, the number of measured reflections was 3955 ($3.42^\circ\le\theta\le31.90^\circ$) with 742 reflections being independent (R_{int} 0.0339). Corrections for Lorentz and polarization effects were carried out and also for absorption with the empirical ψ scan method [35] using the XRAYACS programme [36]. The structures were solved by direct methods and refined by the full-matrix least-squares procedure based on $F2$, using the SHELXL 97 computer programme [37] belonging to the WINGX software package [38]. The scattering factors were taken from Ref. [39]. The quality of the crystals allowed us to determine the hydrogen positions in the structure. The coordinates of hydrogen atoms were calculated from different Fourier maps. The metal ions (Co and Cu) were coupled refined and oxygen atoms were assigned anisotropic and isotropic thermal parameters for $Co_2(OH)AsO_4$ and $Co_{1.7}Cu_{0.3}(OH)AsO_4$, respectively (see Table 2). The results obtained for non-sustituted phase are in good agreement with the crystal structure solved by Seller et al. [19] and high resolution neutron powder diffraction [21]. Final R factors were $R1=0.021$ (all data) [w$R2=0.040$] for $x=0$ and $R1=0.027$ (all data) [w$R2=0.051$] for $x=0.3$. Maximum and minimum peaks in final difference synthesis were 0.701, -0.757 e Å^{-3} and 1.604, -1.080 e Å^{-3} for $x=0$ and 0.3 composition, respectively. The goodness of fit on $F2$ was 0.903 for $Co_2(OH)AsO_4$ and 0.975 for $Co_{1.7}Cu_{0.3}(OH)AsO_4$. All drawings were made using the ATOMS programme [40]. Fractional atomic coordinates and equivalent isotropic thermal parameters are shown in Table 2. In the $Co_{1.7}Cu_{0.3}(OH)AsO_4$ compound, the results of the structural refinement show a preference of the Cu(II) ions for the penta-coordinated position. The Cu(II) cation occupies approximately 24(2)% of the $M(1)$–O_5 sites, whereas only 12(2)% of the $M(2)$–O_6 polyhedra are occupied by this cation; see Table 2. Selected bond distances are given in Table 3.

Table 1
Crystal data, details of data collection, and structure refinement for the $Co_{2-x}Cu_x(OH)AsO_4$ ($x=0$ and 0.3) hydroxi-arsenates.

Formula	$HAsCo_2O_5$	$HAsCo_{1.7}Cu_{0.3}O_5$
Molecular weight ($gmol^{-1}$)	273.79	275.17
Crystal system	Rhombic	Rhombic
Space group	*Pnnm* (*no.* 58)	*Pnnm* (*no.* 58)
a (Å)	8.277(2)	8.3156(9)
b (Å)	8.559(2)	8.523(2)
c (Å)	6.0387(10)	6.0468(7)
V (Å)^3	427.8(2)	428.6(1)
Z	4	4
ρ_{calc}	4.251	4.265
F (000)	512	514
T, K	293	293
μ (mm^{-1})	15.337	15.637
Radiation, λ(Mo $K\alpha$) (Å)	0.7107	0.7107
Range of θ (deg.)	$4.93^\circ\le\theta\ge26.04^\circ$	$3.42^\circ\le\theta\ge31.90^\circ$
Limiting indices	$-10<h<10$, $-9<k<9$, $-7<l<7$	$-11<h<11$, $-12<k<9$, $-8<l<8$
R [$I\ge2\sigma(I)$]	$R1=0.021$, $wR2=0.040$	$R1=0.027$, $wR2=0.051$
R [all data]	$R1=0.041$, $wR2=0.044$	$R1=0.044$, $wR2=0.056$
Goodness of fit	0.903	0.975

[a] $R1=\sum\left|\left|(|F_o|-|F_c|)\right|/\sum|F_o|$; $wR2=\sum|w(|F_o|^2-|F_c|^2)^2|/\sum|w(|F_o|^2)^2|^{1/2}$; $w=\left|1/(\left|\sigma^2||F_o|^2\right)+(x\rho)^2\right|$; where $\rho=|(|F_o|^2)+2|F_o|^2|/3$

where $x=0.0399$ for $Co_2(OH)AsO_4$ and $x=0.0264$ for $Co_{1.7}Cu_{0.3}(OH)AsO_4$.

Table 2
Occupation factor (K), Fractional atomic coordinates and equivalent isotropic parameters U_{eq} for $Co_2(OH)AsO_4$ and $Co_{1.7}Cu_{0.3}(OH)AsO_4$ (ESD in parenthesis).

Atom	K	x/a	y/b	z/c	U_{eq} (Å)^2 [a]
$Co_2(OH)AsO_4$					
Co(1)	0.50	0.3654(1)	0.3652(1)	0.5000	0.93(1)
Co(2)	0.50	0.5000	0.0000	0.2468(2)	0.93(1)
As	0.50	0.2476(1)	0.2449(4)	0.0000	0.68(1)
O(1)	0.50	0.1026(5)	0.1075(6)	0.0000	1.05(1)
O(2)	0.50	0.4232(4)	0.1475(6)	0.0000	1.61(1)
O(3)	1.00	0.2285(3)	0.3621(5)	0.2229(5)	1.05(1)
O(4)	0.50	0.3904(5)	0.1277(7)	0.5000	1.94(1)
H	0.50	0.3974(5)	0.1075(6)	0.5000	1.00
$Co_{1.7}Cu_{0.3}(OH)AsO_4$					
Co(1)	0.38(1)	0.3668(1)	0.3657(1)	0.5000	1.34(1)
Cu(1)	0.12(1)	0.3668(1)	0.3657(1)	0.5000	1.34(1)
Co(2)	0.44(3)	0.5000	0.0000	0.2474(1)	1.34(1)
Cu(2)	0.06(1)	0.5000	0.0000	0.2474(1)	1.34(1)
As	0.50	0.2470(1)	0.2453(1)	0.0000	1.46(1)
O(1)	0.50	0.1058(4)	0.1062(4)	0.0000	1.28(1)
O(2)	0.50	0.4237(4)	0.1468(4)	0.0000	1.28(1)
O(3)	1.00	0.2269(3)	0.3625(3)	0.2235(4)	1.28(1)
O(4)	0.50	0.3924(4)	0.1288(4)	0.5000	1.28(1)
H	0.50	0.3944(8)	0.1002(9)	0.5000	1.00

[a] $U_{eq}=(1/3)\ (U_{11}+U_{22}+U_{33})$.

3. Results and discussion

3.1. Crystal structure

The crystal structure of the $Co_{2-x}Cu_x(OH)AsO_4$ ($x=0$ and 0.3) compounds along the [0 1 0] direction is illustrated in Fig. 1. The topological description of $Co_{1.7}Cu_{0.3}$ $(OH)AsO_4$ is similar to that of $Co_2(OH)AsO_4$, with the partial Co(1) and Co(2) substituted by Cu(1) and Cu(2), respectively. Of the two different crystal metal positions, $M(1)$ is fivefold coordinated by O(1), O(3) and O(4)H oxygen atoms in approximately trigonal bipyramidal geometry, and $M(2)$ exhibits a distorted octahedral geometry, coordinated by O(2), O(3) and O(4)H oxygen atoms (see Table 3). The octahedra sharing the O(2)–O(2) and the O(4)H–O(4)H edges give rise to linear chains propagated along the z-axis. In addition, the two trigonal bypiramids constitute a dimer sharing the O(1)–O(1) edge. The chain of octahedra, the dimeric unit and the AsO_4 tetrahedral groups share corners thereby forming a three-dimensional network (see Fig. 1).

In the $Co_{1.7}Cu_{0.3}(OH)AsO_4$ phase, the cobalt and copper $M(2)$ atoms are set out in elongated octahedra, with two long apical bond distances, $M(2)$–$O(3)^i$ of 2.226(1) Å, and four shorter equatorial links, $M(2)$–O(2) of 2.074(2) Å and $M(2)$–O(4)H of 2.064(2) Å (see Table 3). The main structural difference between the doped and undoped compounds occurs in the $M(2)O_4(OH)_2$ (M=Co and Cu) octahedral distortions. The doped phase exhibits a higher distortion in the equatorial plane O(2), O(2), O(4)H, and O(4)H due to the Jahn–Teller effect of the Cu(II) ion giving rise to higher angle values, [$M(2)$–O(4)H–$M(2)$] and [$M(2)$–O(2)–$M(2)$], in the octahedral chains. The $M(1)$ atoms are fivefold coordinated by oxygen atoms, where the equatorial $M(1)$–$O(1)^{ii}$ and $M(1)$–O(3) bond distances are 2.065(3) and 2.037(2) Å, respectively,

Table 3
Selected bond distances for $Co_2(OH)AsO_4$ and $Co_{1.7}Cu_{0.3}(OH)AsO_4$ (ESD in parenthesis). Symmetry code: *i*=½−*x*, *y*−1/2, ½−*z*; *ii*=1/2−*x*, ½+*y*, 1/2−*z*; *iii*=*x*−1/2, ½−*y*, *z*−1/2; *iv*=−*x*, −*y*, 1−*z*; *v*=*x*−1/2, ½−*y*, 1/2−*z*; vi=−*x*, −*y*, −*z*; *vii*=*x*, *y*,−*z*; *viii*=*x*, *y*, 1/2−*z*.

$M(2)O_4(OH)_2$ octahedron			$M(1)O_4(OH)$ trigonal bipyramid			AsO_4 tetrahedron		
	***x*=0**	***x*=0.3**		***x*=0**	***x*=0.3**		***x*=0**	***x*=0.3**
Bond distances (Å)								
M(2)–O(2)	2.082(4) x2	2.074(2) x2	*M*(1)–O(4)H	2.044(6)	2.029(3)	As–O(1)	1.680(5)	1.682(3)
M(2)–O(4)H	2.059(4) x2	2.064(2) x2	*M*(1)–O(1)^{ii}	2.090(6)	2.065(3)	As–O(2)	1.676(4)	1.693(3)
M(2)–O(3)^{i}	2.234(3) x2	2.226(1) x2	*M*(1)–O(1)^{iii}	1.977(4)	1.984(3)	As–O(3)	1.685(3) x2	1.689(2) x2
			M(1)–O(3)	2.023(3) x2	2.037(2) x2			
Bond angles (deg.)						AsO_4 tetrahedron		
O(2)–*M*(2)–O(2)	87.0(1)	86.5(1)	O(1)H–*M*(1)–O(1)^{iii}	75.9(3)	76.8(3)	O(1)–As–O(2)	105.7(2)	104.5(2)
O(2)–*M*(2)–O(3)H	97.0(1)	96.9(2)	O(1)H–*M*(1)–O(3)	94.8(2) x2	94.3(2) x2	O(1)–As–O(3)	110.4(1) x2	110.7(1) x2
O(2)–*M*(2)–O(3)^{v}	89.8(2)	89.6(3)	O(1)^{ii}–*M*(1)–O(4)^{iii}	166.9(4)	167.7(4)	O(2)–As–O(3)	112.2(3) x2	112.4(4) x2
O(2)–*M*(2)–O(4)^{i}	171.1(2)	171.6(2)	O(1)^{iii}–*M*(1)–O(3)	123.9(3) x2	124.6(2) x2	O(3)–As–O(3)^{viii}	105.9(4)	106.1(2)
O(3)H–*M*(2)–O(3)H^{vi}	170.6(2)	170.9(4)	O(3)^{ii}–*M*(1)–O(4)	92.5(1) x2	92.6(3) x2			
O(3)H–*M*(2)–O(4)^{i}	81.3(2)	82.0(2)						
O(3)H–*M*(2)–O(4)^{v}	91.8(2)	91.3(2)						
O(4)^{i}–*M*(2)–O(4)^{v}	85.8(2)	85.7(1)						

whereas the apical *M*(1)–O(1)^{iii} and *M*(1)–O(4)H bond distances are 1.984(3) and 2.029(3) Å, respectively. No major differences between the O–*M*–O bond angles of the two crystal structures were detected (see Table 3). This result is probably due to the small copper ion occupation (12% of the *M*(2)–O_6 polyhedra). As was observed in the octahedral geometry, the $Co_{1.7}Cu_{0.3}$ compound presents a lower degree of distortion of the *M*(1)O_4(OH) polyhedra. The copper occupation (24% of the *M*(1)–O_5 polyhedra) does not seem to be enough to produce greater *M*(1)–O distances, which are normally associated to the Jahn–Teller effect.

On the other hand, the axial direction of the octahedra, O(3)–*M*(2)–O(3), shows different tilt angles with respect to the *x*-axis, 34.93° and 36.44° for *x*=0 and 0.3, respectively. These factors cause the decrease of the *b* parameter together with an increase in the *a* parameter for the doped phase (see Table 1) is in good agreement with that observed in the $Co_{2-x}Cu_x(OH)PO_4$ solid solution [25]. In addition, the distorted trigonal bipyramidal geometry in both compounds presents two types of similar distances, one of them with four distances of approximately 2.04 Å and another one close to 1.99 Å (see Table 3). The *M*(1)–O(1)–*M*(1) angle in the dimers is almost similar (104°) in both compounds. Finally, the arsenate group partakes in four As–O–[2 × *M*] bonds [each bond links to two *M*(1) and/or *M*(2)], resulting in a condensed structure without any identifiable channels or pores. The three As–O bond distances in the $Co_{1.7}Cu_{0.3}(OH)AsO_4$ phase are slightly higher than that of the non-substituted cobalt hydroxi-arsenate compound, but their O–As–O angles are similar in both compounds and near to the theoretical 109° tetrahedral angle.

3.2. Spectroscopic measurements

The IR spectra of the title compounds show three distinct features corresponding principally to the vibrations of the hydroxide and arsenate groups [31,41,42] (Supplementary material, Fig. S.1). In both phases there is a sharp band at approximately 3540 cm^{-1} together with a broad band between 3300 and 3500 cm^{-1} attributed to a bridging O–H group. The bands observed in the 700–1000 cm^{-1} region are due to the stretching vibration modes of the AsO_4^{3-} groups. The asymmetrical stretching mode [ν_{as} (As–O)] appears at frequencies 840 and 825 cm^{-1} for $Co_2(OH)AsO_4$ and at 830 and 810 cm^{-1} for $Co_{1.7}Cu_{0.3}$(O-H)AsO_4. The symmetrical stretch [ν_s (As–O)] is detected at frequencies 620 and 610 cm^{-1} for the cobalt and cobalt–copper phases, respectively. The small shift of all these signals at lower wavelengths in the substituted arsenate is probably due to the presence of Cu(II) ions in the structure is in good agreement with the structural results were higher As–O distances were observed (see Table 3). The asymmetrical deformation vibrations [δ_{as}(O–As–O)] of both compounds show practically the same aspect ratio with signals at 540 and 490 cm^{-1} for the cobalt hydroxi-arsenate and at 535 and 485 cm^{-1} for the cobalt–copper phase. These bands appear at frequencies similar to those observed for other arsenate phases but at frequencies lower than those observed for the homologous hydroxi-phosphates, as correspond to shorter P–O bond distances in the latter compounds [30,31,41,42].

The absorption bands observed in the diffuse reflectance spectra of Co_{2-x} $Cu_x(OH)AsO_4$ (*x*=0 and 0.3) correspond to the two different chromophores of the Co(II) ions, with octahedral and trigonal bipyramidal symmetries (Supplementary material, Fig. S.2). For the CoO_6 chromophore of $Co_2(OH)AsO_4$, the three spin-allowed transitions $^4T_{1g}\rightarrow{}^4T_{2g}$, $^4A_{2g}$ and $^4T_{1g}$(P) appear at the following frequencies: ν_1=7700, ν_2=15500 and ν_3=18020 cm^{-1} [29] near to the two observed in the cobalt–copper substituted phase (ν_2=16100 and ν_3=18120 cm^{-1}). The Dq and B Racah parameters, calculated by fitting the experimental frequencies to an energy level diagram for an octahedral d^7 system [43], for the non-substituted phase are 770 and 815 cm^{-1}, respectively. However, the deformation of the cobalt absorption bands due to the presence of copper ion in octahedral geometry, with spin-allowed chromophore transition $^4B_1(dx^2-y^2)\rightarrow{}^4A''_1$ at frequency of 8550 cm^{-1}, complicates the determination of the Dq and B parameters in $Co_{1.7}Cu_{0.3}(OH)AsO_4$. The effects of the low symmetry and the spin–orbit coupling for the Co(II) ions ($\lambda=-180$ cm^{-1} for the free ion) in an octahedral geometry remove the degeneracy of the cubic $^4T_{1g}$ term, resulting in a doubled ground state. In this way, the system may be described as having an effective spin *S*=½ at low temperatures (*T*<30 K). The CoO_5 trigonal bipyramidal chromophores of $Co_2(OH)AsO_4$ exhibit bands at frequencies 5500, 6250, 7000, 10870, 16000 and 19800 cm^{-1} attributed to the $^4A'_2\rightarrow{}^4A''_1$, $^4A''_2$; $^4E''$; $^4E'$; $^4A'_2$(P) and $^4E''$(P) spin-allowed transitions [29]. In the $Co_{1.7}Cu_{0.3}(OH)AsO_4$ phase only bands at frequencies of 6950, 10700 and 19850 cm^{-1} were observed (Supplementary material, Fig. S.2).

In both hydroxi-arsenate phases the position of these bands are in the ranges usually found for octahedral and trigonal bipyramidal coordinated Co(II) compounds [23,24]. The assignments are in good agreement with those obtained from electron spin resonance spectroscopy carried out in the $Zn_2(OH)PO_4$ and $Mg_2(OH)AsO_4$ isomorphous phases doped with Co(II) ions [23,43].

3.3. Magnetic measurements

DC magnetic susceptibility measurements from 2 to 300 K at 1 kOe after cooling in absence (zero field cooling, ZFC) of the applied field for $Co_{1.7}Cu_{0.3}(OH)AsO_4$, together with the magnetic data of the non-substituted phase are shown in Fig. 2. The molar magnetic susceptibility of $Co_{1.7}Cu_{0.3}(OH)AsO_4$ increases from room temperature as the temperature decreases and reaches a rounded maximum at approximately 40 K. At low temperatures, another magnetic signal at 20 K appears and a new inflection point close to 7 K is observed. This magnetic behaviour is significantly different from those observed in the $Co_2(OH)AsO_4$ compound (see Fig. 2), where the χ_m arrives at a rounded maximum at approximately 30 K, followed by a strong increase in magnetic signal below 19 K and a new inflection point close to 6 K [21]. This effect can be attributed to the spin changes on the magnetic behaviour as a result of the substitution of Co^{2+} ($S=3/2$) by Cu^{2+}($S=1/2$) ions [44]. The comparison with its homologous hydroxi-phospate $Co_{1.7}Cu_{0.3}(OH)PO_4$ compound shows significant differences where only one maximum at 65 K associated to the three-dimensional antiferromagnetic interactions appears [25].

At temperatures higher than 100 K, the magnetic susceptibility data of $Co_{1.7}Cu_{0.3}(OH)AsO_4$ follow a classical Curie–Weiss law with an extrapolated Curie temperature, θ_p, near -64 K and Curie constants of 3.05 emu K/mol Oe. These values are close to -62 K and 3.26 emu K/mol Oe obtained in the $Co_2(OH)AsO_4$ compound and other cobalt-based $Co_2(OH)(PO_4)_{1-x}(AsO_4)_x$ phases [24]; this is consistent with the results reported in the literature for high spin d^7 Co^{2+} ions [45]. The negative Weiss temperature together with the decrease of the effective magnetic moment observed when the temperature is lowered indicates that the major magnetic interactions are antiferromagnetic. The change of curvature of the susceptibility at $T_N \approx 20$ K in $Co_{1.7}Cu_{0.3}(OH)AsO_4$ can be attributed to the onset of AF order, as will be described later from heat capacity data. These magnetic results are in good agreement with those of the non-substituted phase, where an exhaustive description can be found in Ref. [21].

The temperature dependence of the ZFC-FC curve in $Co_{1.7}Cu_{0.3}(OH)AsO_4$ phase is reversible and follows the same pathway independently of how the temperature is approached [see inset of Fig. 2]. On the other hand, the data of $Co_2(OH)AsO_4$ do not show any difference above 15 K. Below this temperature, the curves show a small splitting attributed to the existence of a small ferromagnetic component [21]. These results indicate that the introduction of Cu(II) ($S \approx ½$) ions favours the spin decompensations in the $Co_{1.7}Cu_{0.3}(OH)AsO_4$ phase, giving rise to the breakdown of ferromagnetic coupling observed in the $Co_2(OH)AsO_4$ compound [24].

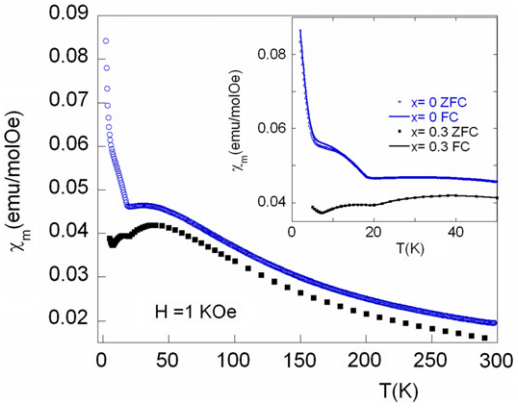

Fig. 2. Thermal evolution of the molar magnetic susceptibility (χ_m) at 1 kOe for $Co_2(OH)AsO_4$. The inset shows low temperature ZFC-FC measurements at 1 kOe.

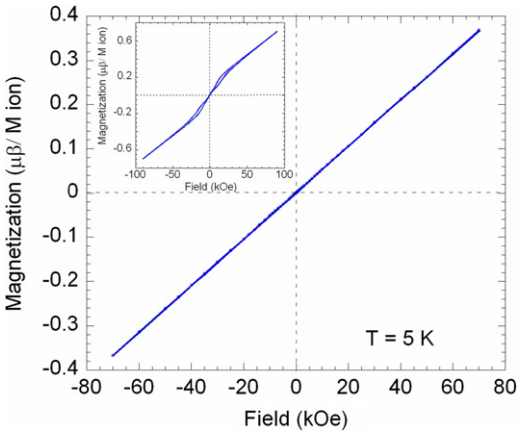

Fig. 3. Magnetization vs. applied magnetic field at 5 K for $Co_{1.7}Cu_{0.3}(OH)AsO_4$ and $Co_2(OH)AsO_4$ (inset).

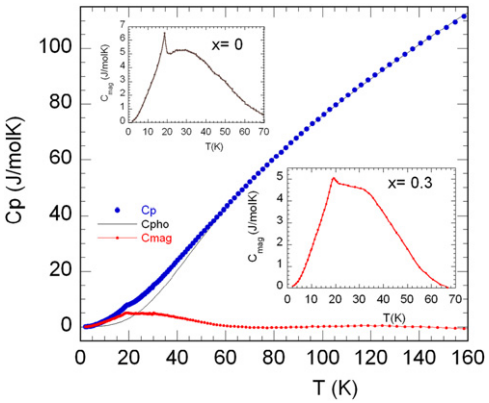

Fig. 4. Specific heat of $Co_{1.7}Cu_{0.3}(OH)AsO_4$ between 1.8 and 160 K. Experimental data (blue full dots), estimated phonon contribution (black solid line), and magnetic contribution (red dots). Upper and lower insets show the magnetic specific heat of $Co_2(OH)AsO_4$ and $Co_{1.7}Cu_{0.3}(OH)AsO_4$, respectively, between 1.8 and 70 K. (For interpretation of the references to color in this figure legend, the reader is referred to the web version of this article.)

The magnetic field dependence of magnetization at 5 K is shown in Fig. 3. As can be seen, the magnetization curve of $Co_{1.7}Cu_{0.3}(OH)AsO_4$ phase shows a linear dependence in the whole applied field range studied. Furthermore, the magnetization shows an absence both of a ferromagnetic component [in good agreement with dc magnetic susceptibility measurements (see inset of Fig. 2)] and metamagnetic transition, in the entire applied field investigated. In contrast, the dependence on the magnetization with applied magnetic field in the non-substituted arsenate follows, between 3.5 and 40 kOe, a process in stages characteristic of a metamagnetic transition (see inset Fig. 3) and a small irreversibility with H_{max} of 4.5 kOe [21]. Finally, it is worth mentioning that the value of magnetization at 70 kOe is lower than the non-substituted phase (0.4 μ_B/M ion) and quite different from the theoretical saturation magnetic moment for this compound (3.0 μ_B/mol). Besides, at 70 kOe, the saturation is not reached indicating the existence of a strong anisotropy as was observed in the homologous $(Co,M)_2(OH)PO_4$ (M=Mn, Ni and Cu) hydroxi-phosphates [24–28].

3.4. Heat capacity measurements

The specific-heat measurements of $Co_{1.7}Cu_{0.3}(OH)AsO_4$ between 1.8 and 150 K in the absence of an external magnetic field are shown in Fig. 4. An enlargement around the magnetic transition for the non-substituted phase has also been included

for comparison (see inset of Fig. 5). Calorimetric measurements of both hydroxi-arsenate compounds reveal a small maximum (ΔC_p=2 and 0.2 J/Kmol) centred at 18.6 and 19.8 K for x=0 and 0.3, respectively (see Fig. 5). This anomaly does not have the typical appearance of a second order transition of λ, but it can be associated with the establishment of a three-dimensional antiferromagnetic ordering. Besides, the temperatures at which these anomalies appear are consistent with a rounded maximum ($T \approx 20$ K) observed in the magnetic susceptibility measurements of $Co_{1.7}Cu_{0.3}(OH)AsO_4$ (see Figs. 2 and 5).

On the other hand, no anomalies were observed above 30 and below 10 K (see Fig. 4), which prompted us to propose that the magnetic contributions at around 40–7 K detected in the magnetic susceptibility measurements (see Fig. 2) are not of a long-range type (implying a disordered magnetism). Finally, above the magnetic transition, the molar heat capacity (C_p) increases continuously due to the phonon contribution and does not show any tendency to saturation even up to room temperature, where the value of C_p is 160 and 166 J/Kmol for x=0 and 0.3, respectively. These values are well distant from the expected amount according to the Dulong and Petit law (near to 225 J/kmol) [46].

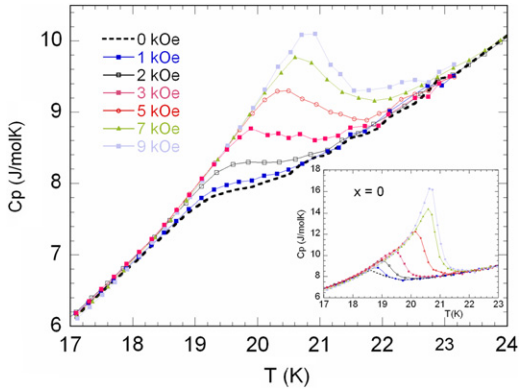

Fig. 5. Enlargement around the Neel temperature of specific heat as a function of temperature in the presence of external magnetic fields ($H \leq 90$ kOe) of $Co_{1.7}Cu_{0.3}(OH)AsO_4$ and $Co_2(OH)AsO_4$ (inset).

This result is probably due to the presence of light atoms with very high excitation energy [21,23].

The experimental magnetic heat capacity (C_{pmag}) contribution in $Co_{1.7}Cu_{0.3}(OH)AsO_4$ was obtained subtracting the inferred phonon contribution (C_{ppho}) from the measured specific heat (see the lower inset of Fig. 4). The exact calculation of C_{ppho} is difficult due to the absence of a suitable non-magnetic isomorphous compound. As it was satisfactorily used for $Co_2(OH)AsO_4$ [21], an estimation of C_{ppho} was obtained using the Debye model [47] and considering the existence of two Debye temperatures, the smaller one (θ_1) associated to the heavy ions (n_1) such us Co, Cu and As and the higher one (θ_2) associated to the O and H light ions (9–n_1). The best fit to the experimental data for $T \geq 60$ K is obtained for θ_1=264 K, θ_2=980 K and n_1=3.6 ions, showing a decrease of the Debye temperature with respect to the non-substituted phase (θ_1=270 K, θ_2=1048 K) in good agreement with the hydroxi-phosphate $(Co,Cu)_2(OH)PO_4$ solid solution [25]. Besides, apart from the small maximum (smaller that the non-substituted phase) associated with the three-dimensional magnetic order observed around 19 K, another anomaly like a shoulder circa 30 K appears in both title compounds (see insets of Fig. 4). This kind of broad maximum, also shown in magnetic measurements, could come from different origins: (i) bidimensional magnetic ordering, (ii) short-range magnetic interactions or (iii) a crystalline electrical field [21]. One effect of this maximum is that the magnetic entropy (not shown) tends to saturate well above the magnetic transition, at around 60 K in both compounds, with values of 8.2 and 7.3 J/kmol for $Co_2(OH)AsO_4$ and $Co_{1.7}Cu_{0.3}(OH)AsO_4$, respectively.

The results of the heat capacity measurements of $Co_{1.7}Cu_{0.3}(OH)AsO_4$ carried out in the presence of several magnetic fields are shown in Fig. 5. The curves reveal that the anomaly around 19 K, associated to the three-dimensional ordering, grows and moves toward higher temperatures (circa 1.5 K) as the applied field increases thus becoming better defined. This anomalous magnetic behaviour is not expected in antiferromagnetic transitions where the anomaly, due to the effect of the magnetic field, becomes rounder and decreases in height. In our case, as was observed in $Co_2(OH)AsO_4$ (see inset of Fig. 5), it could be associated with the induction of commensurability in an incommensurate magnetic

Table 4

Selected geometrical parameters obtained from single crystal X-ray diffraction, bond lenghts (Å) and angles (deg) related to the possible magnetic superexchange pathways for $Co_2(OH)AsO_4$ and $Co_{1.7}Cu_{0.3}(OH)AsO_4$ phases.

$Co_2(OH)AsO_4$	Direct distance M–M (Å)	Length of exchange pathway	Angles (deg.)			
			M–O–M	M–O–As	O–As–O	As–O–M
M(1)–O(1)–M(1)	3.20	4.10	104.6			
M(1)–O(1)–As–O(3)–M(1)	5.57	7.53		127.0	110.4	128.0
M(1)–O(4)H–M(2)	3.65	4.12	124.4			
M(1)–O(3)–M(2)	**3.56**	**4.25**	**114.6**			
M(1)–O(3)–As–O(2)–M(2)	3.56	7.51		128.0	112.0	124.6
M(2)–O(4)H–M(2)	3.06	4.16	94.3			
M(2)–O(2)–M(2)	2.98	4.11	93.8			
M(2)–O(2)–As–O(3)–M(2)	5.93	7.61		125.0	112.2	117.3
$Co_{1.7}Cu_{0.3}(OH)AsO_4$	Direct distance M–M (Å)	Length of exchange pathway	Angles (deg.)			
			M–O–M	M–O–As	O–As–O	As–O–M
M(1)–O(1)–M(1)	3.19	3.98	103.2			
M(1)–O(1)–As–O(3)–M(1)	5.49	7.40		127.5	110.8	127.6
M(1)–O(4)H–M(2)	3.65	4.11	124.8			
M(1)–O(3)–M(2)	**3.57**	**4.26**	**115.2**			
M(1)–O(3)–As–O(2)–M(2)	3.65	7.45		127.5	112.4	125.0
M(2)–O(4)H–M(2)	3.08	4.16	96.2			
M(2)–O(2)–M(2)	3.02	4.10	95.5			
M(2)–O(2)–As–O(3)–M(2)	5.95	7.64		124.9	112.4	117.4

structure by the effect of the magnetic field [21]. In fact, preliminary neutron diffraction data confirm the existence of an incommensurate magnetic structure in $Co_{1.7}Cu_{0.3}(OH)AsO_4$ at low temperatures.

3.5. Magnetostructural correlations

The main magnetic exchange pathways present in the title compounds are shown in Table 4 and Fig. 6. For both hydroxiarsenates, direct interactions are not negligible taking into account their shorter metal–metal distances, between 2.9 and 3.6 Å. Considering the angles in $Co_{1.7}Cu_{0.3}(OH)AsO_4$, both ferro and antiferromagnetic interactions should be observed [48]. However, the nature of some magnetic interactions can be modified favouring the antiferromagnetic pathways due to the substitution of approximately 15% of Co(II) (d^7) ($S=3/2$) by Cu(II) (d^9) ($S=1/2$) in the $Co_2(OH)AsO_4$ framework [21] and the slight preference of the Cu^{2+} ions for the $M(1)$ trigonal bypiramidal dimers.

On the other hand, considering that the unpaired electrons in the Co^{2+} and Cu^{2+} ions are in the d_{z^2} and $d_{x^2-y^2}$ orbitals, respectively, the propagation of the magnetic interactions is disfavoured in the dimers and both the ferromagnetic component and the geometrical spin frustration decrease in the $Co_{1.7}Cu_{0.3}(OH)AsO_4$ phase. In contrast, a spin frustration between chains and dimers in $Co_2(OH)AsO_4$ together with the appearance of ferromagnetic arrangements between the Co(2) octahedral chains and Co(1) trigonal bipyramidal dimers along the *c*-axis-modulated antiferromagnetic between subnets in direction *b* are observed [21].

The possible exchange pathways in the $Co_{2-x}Cu_x(OH)AsO_4$ ($x=0$ and 0.3) phases are (i) direct interactions involving $M(1)$ and $M(2)$ sublattices, which should lead to antiferro–magnetic couplings; (ii) superexchange M–O–M interactions from edge-sharing both in the $[M(1)_2O_6(OH)_2]$ trigonal bipyramidal dimers and $[M(2)O_4(OH)_2]$ octahedral chains, whose angles range from 103.2° to 104.6° and from 93.8° to 96.2°, respectively, leading to ferromagnetic interactions in both compounds (see Table 4); (iii) superexchange $M(1)$–O(3)-$M(2)$ and $M(1)$–O(4)H–$M(2)$ interactions between dimers and their neighbouring chains that could give rise to ferro or antiferro–magnetic couplings depending on the magnetic exchange angle and favouring the antiferromagnetic ones with the presence of Cu(II). The connecting point of the polyhedra through the OH group, $M(1)$–O(4)H–$M(2)$, shows angles close to 125° for both compounds giving rise to antiferro–magnetic couplings. These results are in good agreement with those obtained by high resolution neutron powder diffraction of the $Co_2(OH)AsO_4$ phase [21].

It is worth mentioning that the $M(1)$–O(3)–$M(2)$ (M=Co and Cu) magnetic exchange pathway (for ferromagnetic interactions through the *xz* plane) is being considered essential in the competition between dimers and chains in order to lead a magnetic frustration system with an incommensurate phase with antiferromagnetic interactions sinusoidal amplitude modulated in the $Co_2(OH)AsO_4$ phase [21]. As can be seen in Table 4, the substitution of up to 15% of Co^{2+} by Cu^{2+}, $Co_{1.7}Cu_{0.3}(OH)AsO_4$, does not affect this orthogonal accidental angle, $M(1)$–O(3)–$M(2)$ angle value of 115.2° enough, to force changes in the sense of the magnetic interactions. Moreover, the substitution of AsO_4^{3-} by PO_4^{3-} anions in the $Co_2(OH)XO_4$ (X=P and As) phases substantially modifies the magnetic exchange Co(1)–O(3)–Co(2) angle from 114.6° to 107° for the arsenate and phosphate, respectively, ensuring the cooperativeness of the freezing process associated to a spin glass-like state of the $Co_2(OH)PO_4$ phase [23].

A final possible exchange pathway is (iv) superexchange antiferromagnetic interactions through the $|AsO_4|$ groups, which are linked to the $|M(1)O_5|$ and $|M(2)O_6|$ polyhedra in three dimensions. The superexchange M–O–As–O–M interactions (see Fig. 6) could lead to a frustration in the structure, which can favour an incommensurate magnetic structure at low temperature, as previously discussed. This last pathway also allows one to propagate the magnetic interactions giving rise to a complex three-dimensional magnetic system.

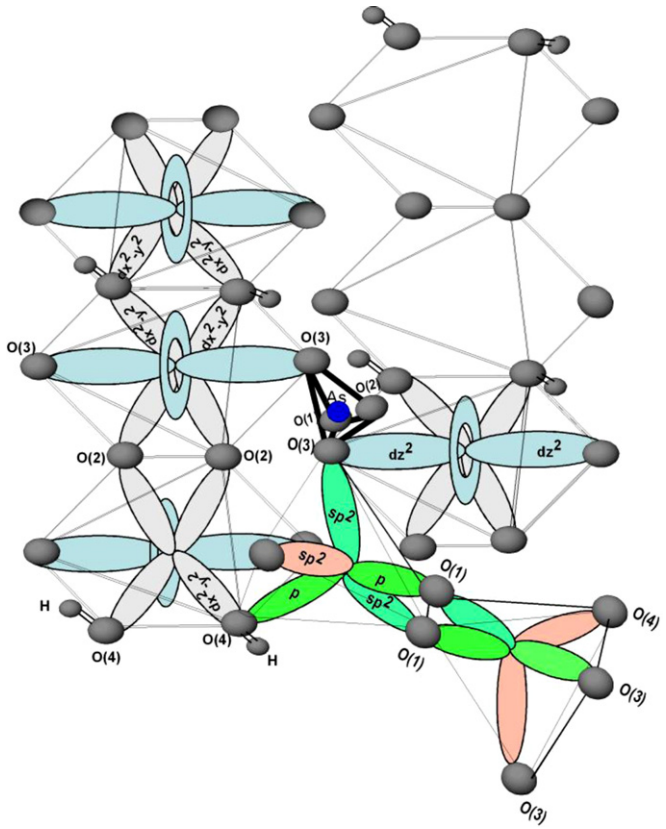

Fig. 6. Schematic view of the exchange pathways for $Co_{2-x}Cu_x(OH)AsO_4$ ($x=0$ and 0.3). Orbitals involved in the pathways via oxygen bridges of edge-sharing, vertex oxygen bridges, and arsenate groups are represented.

4. Conclusions

A new compound, $Co_{1.7}Cu_{0.3}(OH)AsO_4$, with adamite-type structure has been synthesized under hydrothermal conditions and characterized by single crystal X-ray diffraction. The distribution of the Cu(II) ions in the $M(1)$ and $M(2)$ sites shows a preference (66%) for the trigonal bipyramid dimers. Single crystal X-ray diffraction data of $Co_{1.7}Cu_{0.3}(OH)AsO_4$ show that a distortion of the octahedral subunit is greater than the non-substituted phase due to the presence of Cu(II). This factor causes the decrease in *b* parameter together with an increase in *a* parameter is in good agreement with the $Co_{2-x}Cu_x(OH)PO_4$ solid solution. The magnetic behaviour of the $Co_{1.7}Cu_{0.3}(OH)AsO_4$ phase shows the existence of predominant antiferromagnetic interactions. The spin decompensation originated by the substitution of Co^{2+} ($S=3/2$) by Cu^{2+} ($S=1/2$) play an important role in the irreversibility process, with their effect on the ZFC-FC measurements being clearly different from that observed in $Co_2(OH)AsO_4$. This fact gives rise to a disappearance of any ferromagnetic component, although the 3D ordering is maintained. It can be explained by both the presence of the Cu^{+2} (d^9) ions in the octahedral and bipyramid trigonal geometries decreasing frustration between them and the presence of the unpaired electrons in the $d_{x^2-y^2}$ orbitals. Specific heat data for the $Co_{1.7}Cu_{0.3}(OH)AsO_4$ phase support the evidence of the three-dimensional antiferromagnetic ordering between M^{2+} (M=Co and Cu) ions in the low

temperature transition and the existence of a strong magnetic anisotropy. Besides, an unusual effect in the specific heat with the magnetic field is observed. The weak maximum associated to the three dimensional ordering grows with the field, it becoming better defined. A possible explanation for this behaviour is that the effect of the magnetic field is to induce a change in the type of magnetic structure from incommensurate to commensurate, as was observed in the non-substituted phase.

Acknowledgments

This work was financially supported by Basque Country Government Grant IT-312-07 and by MEC research projects (MAT 2008-06542-c04 and MAT 2010-19442), which we gratefully acknowledge.

Appendix A. Supplementary material

Supplementary data associated with this article can be found in the online version at doi:10.1016/j.jssc.2011.05.060.

References

[1] R.C. Haushalter, L.A. Mundi, Chem. Mater. 4 (1992) 31–48.
[2] A. Clearfield, Chem. Rev. 88 (1998) 125–148.
[3] W.R. Rapoport, C.P. Khattak, Appl. Opt. 27 (1988) 2677–2688.
[4] G.T. Forrest, Laser Focus World 25 (1989) 23–25.
[5] J.M. Rojo, J.L. Mesa, R. Calvo, L. Lezama, R. Olazcuaga, T. Rojo, J. Solid State Chem. 145 (1999) 629–633.
[6] F.S. Xiao, J. Sun, X. Meng, R. Yu, H. Yuan, J. Xu, T. Song, D. Jiang, R. Xu, J. Catal. 199 (2001) 273–281.
[7] X. Meng, K. Lin, X. Yang, Z. Sun, D. Jiang, F.S. Xiao, J. Catal. 218 (2003) 460–464.
[8] W.E. Richmond, Am. Mineral. 25 (1940) 441–479.
[9] G. Raade, M.H. Mladeck, Lithos 12 (1979) 283–287.
[10] G. Raade, C. Rømming, Z. Kristallogr. 177 (1986) 1–13.
[11] H. Strunz, E.H. Nickel, Strunz Mineralogical Tables, 9th ed., E. Scheweizebart'sche Verlagsbuchhandlung, Stuttgart, 2001.
[12] A.G. Nord, P. Kierkegaard, T. Stefanidis, J. Baran, Chem. Commun. Univ. Stockholm. 5 (1988) 841–848.
[13] H. Heritsch, Z. Kristallogr. 99 (1938) 466–479.
[14] G. Cocco, L. Fanfani, P.F. Zanazzi, Z. Kristallogr. 123 (1966) 321–329.
[15] P.B. Moore, J.R. Smyth, Am. Mineral. 53 (1968) 1841–1845.
[16] A. Cordsen, Can. Mineral. 16 (1978) 153–157.
[17] F.C. Hawthrone, Can. Mineral. 14 (1976) 143–148.
[18] K. Toman, Acta Crystallogr. B33 (1977) 2628–2631.
[19] P. Séller, H. Hess, F. Zettler, Neues Jahrb. Mineral. Abh. 334 (1979) 27–34.
[20] H. Riffel, F. Zettler, H. Hess, Neues. Jahrb, Mineral. Monatsh. (1975) 514–517.
[21] I. de Pedro, J.M. Rojo, J. Rodríguez Fernández, M.T. Fernández-Díaz, T. Rojo, Phys. Rev. B 81 (2010) 134431/1–134431/14.
[22] M. Kurmoo, Chem. Soc. Rev 38 (5) (2009) 1353–1379.
[23] J.M. Rojo, J.L. Mesa, L. Lezama, J.L. Pizarro, M.I. Arriortua, J. Rodriguez Fernandez, G.E. Barberis, T. Rojo, Phys. Rev. B 66 (2002) 094406/1–094406/13.
[24] I. de Pedro, J.M. Rojo, J. Rodríguez Fernández, L. Lezama, T. Rojo, Eur. J. Inorg. Chem. (2010) 2514–2522.
[25] I. de Pedro, J.M. Rojo, J.L. Pizarro, J. Rodríguez Fernández, J. Sánchez Marcos, M.T. Fernández-Diaz, M.I. Arriortua, T. Rojo, J. Mater. Chem. 17 (2007) 3915–3926.
[26] A.A. Belik, H.J. Koo, M.H. Whangbo, N. Tsujji, P. Naumov, E. Takayama-Mourachi, Inorg. Chem. 46 (2007) 8684–8689.
[27] I. de Pedro, J.M. Rojo, J.L. Pizarro, J. Rodríguez Fernández, J. Sánchez Marcos, M.T. Fernández-Diaz, M.I. Arriortua, T. Rojo, J. Phys. Condens. Matter. 18 (2006) 3767–3787.
[28] I. de Pedro, J.M. Rojo, L. Lezama, T. Rojo, Z. Anorg. Allg. Chem. 633 (2007) 1847–1852.
[29] J.M. Rojo, J.L. Mesa, J.L. Pizarro, L. Lezama, M.I. Arriortua, T. Rojo, J. Solid State Chem. 132 (1997) 107–112.
[30] W.T.A. Harrison, J.T. Vaughey, L.L. Dussack, A.J. Jacobson, T.E. Martin, G.D. Stucky, J. Solid State Chem. 114 (1995) 151–158.
[31] I. de Pedro, J.M. Rojo, V. Jubera, J. Rodríguez-Fernández, J. Sánchez-Marcos, L. Lezama, T. Rojo, J. Mater. Chem. 14 (2004) 1157–1163.
[32] I. de Pedro, J.M. Rojo, M. Insausti, J.L. Mesa, M.I. Arriortua, T. Rojo, Z. Anorg., Allg. Chem. 631 (2005) 2096–2100.
[33] J.M. Rojo, J.L. Mesa, J.L. Pizarro, L. Lezama, M.I. Arriortua, T. Rojo, Mater. Res. Bull. 31 (1996) 925–934.
[34] J. Rodríguez-Carvajal, FULLPROF program for rietveld refinement and pattern matching analysis of powder patterns, Physica B 192 (1993) 55 and unpublished later versions. The program is a strongly modified version of that described by D. B. Wiles, R.A. Young, J. Appl. Crystallogr. 14 (1981) 149.
[35] A.C.T. North, D.C. Philips, F.S. Mathews, A. Semiempirical, Method of absorption correction. Acta Crystallogr. A24 (1968) 351–359.
[36] A. Chandrasekaran, XRAYACS: Program for Single-Crystal X-ray Data Corrections; Chemistry Department, University of Massachusetts, Amherst, MA, 1998.
[37] G.M. Sheldrick, SHELXS 97: Program for the Solution of Crystal Structures, University of Göttingen, Germany, 1997.
[38] L.J. Farrugia, J. Appl. Crystallogr. 32 (1999) 837.
[39] International Tables for X-ray Crystallography. Kynoch Press: Birmingham, U.K. (Eds.), structures; Shape Software (521 Hidden Valley Road): Kingsport, TN, 1974, vol. IV, pp. 99.
[40] E. Dowty, ATOMS: A computer program for displaying atomic structures; Shape Software (521 Hidden Valley Road): Kingsport, TN, 1993.
[41] K. Nakamoto, Infrared and Raman Spectra of Inorganic and Coordination Compounds, 5th ed., John-Wiley & Sons, New York, 1997.
[42] A.B.P. Lever, Inorganic Electronic Spectroscopy, Second ed., Elsevier Science, Amsterdam, 1984.
[43] M.E. Foglio, M.C. dos Santos, G.E. Barberis, J.M. Rojo, J.L. Mesa, L. Lezama, T. Rojo, J. Phys.: Condens. Matter 14 (2002) 2025–2041.
[44] F. Bassani, Handbook of Condensed Matter Physics. Ed, vol. 5, Elsevier Ltd., Amsterdam, 2005.
[45] (a) K.L. Zhanga, Z. Wangb, H. Huangb, Y. Zhuc, X.Z. You, J. Mol. Struct. 693 (2004) 193–197;
(b) R.L. Carlin, Magnetochemistry, Springer-Verlag, Berlin, Heidelberg, New York, Tokyo, 1986.
[46] A.T. Petit, P.L. Dulong, Ann. Chim. Phys. 10 (1819) 395.
[47] P. Debye, Ann. Phys. 344 (1912) 789.
[48] J.B. Goodenough, Magnetism and the Chemical Bond, Wiley Interscience, New York, 1963.